AIAA Journal
Vol. 48, No. 9, September 2010

Technical Notes

DAMAS2 Using a Point-Spread Function Weakly Varying in Space

Takao Suzuki*
The Boeing Company, Seattle, Washington 98124

DOI: 10.2514/1.J050462

Nomenclature

$\mathcal{F}$ = discrete Fourier transform operator
$\mathcal{F}^{-1}$ = inverse discrete Fourier transform operator
k_c = cutoff wavenumber of the wavenumber Gaussian filter
Q = beam-forming output quantity (source intensity)
$\hat{Q}$ = intermediate output quantity for deconvolution
(x, y) = coordinates on the noise-source map
z = height of the microphone array position from the noise-source map
λ = wavelength
(ξ, η) = coordinates of the source position
σ = standard deviation of the spatial Gaussian filter
$\mathbf{\Phi}$ = two-dimensional spatial Gaussian filter
$\mathbf{\Psi}$ = two-dimensional wavenumber Gaussian filter

Subscripts

conv = conventional beam-forming
psf = point-spread function

I. Introduction

THE resolution of noise-source maps processed using phased-array data has been substantially improved by introducing a deconvolution approach for the mapping of acoustic sources (DAMAS [1]), but its practicality is limited due to high computational cost. Subsequently, an improved algorithm, known as DAMAS2 [2], was developed to reduce the computational cost dramatically. Assuming that the monopole response (i.e., the point-spread function) on the source map is invariant over the entire map, referred to as shift invariant, a discrete Fourier transform and its inverse are introduced for deconvolution in DAMAS2. The drawback is that noise-source maps tend to deteriorate away from the point where we defined the point-spread function. Distortion of the monopole response is often severe in wind-tunnel tests, where there are constraints on the location of the microphone array. This note proposes a method that suppresses such deterioration associated with the shift-invariant assumption for DAMAS2 with minimal extra computational cost.

II. Algorithm Description

We express the monopole response of conventional beam-forming on a two-dimensional source map as

$$Q_{\text{conv}}(\xi, \eta; x, y) \approx Q_{\text{conv}}(0, 0; x - \xi, y - \eta) \equiv Q_{\text{psf}}(x - \xi, y - \eta) \tag{1}$$

where the first set of arguments represents the source position, and the second the point specified on the map. The first equality, denoted as approximation, corresponds to the shift-invariant assumption, and the right hand side defines the point-spread function (at the origin in this section for simplicity).

The idea behind the proposed algorithm is to rectify the distortion of the point-spread function by expanding it as a Taylor series with respect to the source displacement. Here, we express the deconvolution process of DAMAS2 [2] as

$$Q^{(i+1)}(x, y) = \max\left[Q^{(i)}(x, y) + \frac{Q_{\text{conv}}(x, y) - \hat{Q}^{(i)}(x, y)}{\sum\limits_{\text{all points}} Q_{\text{psf}}(x', y')}, 0\right] \tag{2}$$

where the intermediate output is given by

$$\hat{Q}^{(i)}(x, y) = \mathcal{F}^{-1}[\mathcal{F}[Q^{(i)}(x', y')]\mathcal{F}[Q_{\text{psf}}(x', y')]\Psi] \tag{3}$$

and the superscript (i) denotes the iteration counter (the expressions basically follow [3]).

Using the same iteration algorithm, we replace the point-spread function with

$$\begin{aligned} Q_{\text{conv}}(\xi, \eta; x, y) &= Q_{\text{conv}}(0, 0; x - \xi, y - \eta) + \xi \frac{\partial Q_{\text{conv}}}{\partial \xi} \\ &\quad + \eta \frac{\partial Q_{\text{conv}}}{\partial \eta} + \frac{\xi^2}{2}\frac{\partial^2 Q_{\text{conv}}}{\partial \xi^2} + \frac{\eta^2}{2}\frac{\partial^2 Q_{\text{conv}}}{\partial \eta^2} + \xi\eta \frac{\partial^2 Q_{\text{conv}}}{\partial \xi \partial \eta} + \cdots \\ &= Q_{\text{psf}}(x - \xi, y - \eta) - [(x - \xi) - x]\frac{\partial Q_{\text{conv}}}{\partial \xi} - [(y - \eta) \\ &\quad - y]\frac{\partial Q_{\text{conv}}}{\partial \eta} + \frac{[(x - \xi) - x]^2}{2}\frac{\partial^2 Q_{\text{conv}}}{\partial \xi^2} + \frac{[(y - \eta) - y]^2}{2}\frac{\partial^2 Q_{\text{conv}}}{\partial \eta^2} \\ &\quad + [(x - \xi) - x][(y - \eta) - y]\frac{\partial^2 Q_{\text{conv}}}{\partial \xi \partial \eta} + \cdots \end{aligned} \tag{4}$$

where the derivatives are evaluated at $(x - \xi, y - \eta)$ with the source placed at $(\xi, \eta) = (0, 0)$, which is the same as the first term on the right hand side; thus, the first term is equivalent to the point-spread function. The higher terms can be similarly derived. The actual differentiation can be performed by shifting the source point, say from the map center to the adjacent grid point on the source map. Therefore, four extra point-spread functions need to be computed for the first derivatives and another four for the second derivatives using central differencing.

When we use a relatively large domain for the source map, absolute values for the terms in Eq. (4) away from $(\xi, \eta) = (0, 0)$ often become greater for higher orders, causing spurious sources. To suppress such artifacts, we introduce a Gaussian spatial filter:

$$\Phi(x - \xi, y - \eta) \equiv \exp\left[-\frac{(x - \xi)^2 + (y - \eta)^2}{\sigma^2}\right] \tag{5}$$

which is multiplied with the terms other than the leading term in Eq. (4) (i.e., the point-spread function). The deviation σ should be determined so that only the artifacts near the edge of the source map

---

Received 27 January 2010; revision received 7 May 2010; accepted for publication 25 May 2010.

*Acoustics and Fluid Mechanics, P.O. Box 3707, MC 67-ML. Member AIAA.

are eliminated. Hence, the original Taylor-series expansion is modified, but only for the correction terms away from the center.

As a result, Eq. (3) is replaced by

$$\begin{aligned}\hat{Q}(x,y) = \mathcal{F}^{-1}\Bigg[&\mathcal{F}[Q]\bigg(\mathcal{F}[Q_{\mathrm{psf}}] - \mathcal{F}\bigg[(x-\xi)\frac{\partial Q_{\mathrm{conv}}}{\partial \xi}\Phi\bigg]\\
&+ x\mathcal{F}\bigg[\frac{\partial Q_{\mathrm{conv}}}{\partial \xi}\Phi\bigg] - \mathcal{F}\bigg[(y-\eta)\frac{\partial Q_{\mathrm{conv}}}{\partial \eta}\Phi\bigg] + y\mathcal{F}\bigg[\frac{\partial Q_{\mathrm{conv}}}{\partial \eta}\Phi\bigg]\\
&+ \mathcal{F}\bigg[\frac{(x-\xi)^2}{2}\frac{\partial^2 Q_{\mathrm{conv}}}{\partial \xi^2}\Phi\bigg] - x\mathcal{F}\bigg[(x-\xi)\frac{\partial^2 Q_{\mathrm{conv}}}{\partial \xi^2}\Phi\bigg]\\
&+ \frac{x^2}{2}\mathcal{F}\bigg[\frac{\partial^2 Q_{\mathrm{conv}}}{\partial \xi^2}\Phi\bigg] + \mathcal{F}\bigg[\frac{(y-\eta)^2}{2}\frac{\partial^2 Q_{\mathrm{conv}}}{\partial \eta^2}\Phi\bigg]\\
&- y\mathcal{F}\bigg[(y-\eta)\frac{\partial^2 Q_{\mathrm{conv}}}{\partial \eta^2}\Phi\bigg] + \frac{y^2}{2}\mathcal{F}\bigg[\frac{\partial^2 Q_{\mathrm{conv}}}{\partial \eta^2}\Phi\bigg]\\
&+ \mathcal{F}\bigg[(x-\xi)(y-\eta)\frac{\partial^2 Q_{\mathrm{conv}}}{\partial \xi \partial \eta}\Phi\bigg] - x\mathcal{F}\bigg[(y-\eta)\frac{\partial^2 Q_{\mathrm{conv}}}{\partial \xi \partial \eta}\Phi\bigg]\\
&- y\mathcal{F}\bigg[(x-\xi)\frac{\partial^2 Q_{\mathrm{conv}}}{\partial \xi \partial \eta}\Phi\bigg] + xy\mathcal{F}\bigg[\frac{\partial^2 Q_{\mathrm{conv}}}{\partial \xi \partial \eta}\Phi\bigg] + \cdots\bigg)\Psi\Bigg] \qquad (6)\end{aligned}$$

where the iteration counter is omitted for simplicity. Hence, four extra Fourier-transformed terms must be precomputed for the first-order correction, and another ten terms for the second order, but they can be calculated before the iteration so that the extra computational time for the correction terms can be minimized. The rest of the process is the same as DAMAS2 [2].

III. Analysis Based on Model Problems

In the following, the capability of the proposed deconvolution algorithm is demonstrated based on model problems. Here, the wavelength is taken to be the length scale, and the speed of sound to be the velocity scale. The size of the source map is set to be $13\lambda \times 13\lambda$ with a grid spacing of 0.25λ; hence, $53 \times 53 = 2809$ grid points are distributed, unless otherwise noted. To represent a microphone array, 60 observer points are deployed along six spiral arms with a radius of 4λ. This plane of the microphone array is set to be 10λ above the source map; accordingly, the array center is defined as $(x, y, z) = (0, 0, 10\lambda)$.

Two cases are considered below, one in which the source map center is located at the origin, and the other at $(x, y, z) = (3\lambda, 3\lambda, 0)$. The microphone positions relative to the source map for these two cases are drawn in Fig. 1. In both cases, the point-spread function and their derivatives are computed at the map center. The cutoff wavenumber of the filter Ψ in Eqs. (3) and (6) is taken to be $k_c = \sqrt{(2\pi/\Delta x) \times (2\pi/\Delta y)}$, and the standard deviation of the spatial filter Φ to be $\sigma = 5\lambda$ in (5). For all the algorithms, 50 iterations are performed.

To compare the accuracy of the proposed algorithm with that of DAMAS2, the intensity and the centroid of the source distribution detected by these algorithms are calculated as a function of the source position. For both microphone distributions, a monopole source with unit strength is shifted diagonally by an increment of $\lambda/\sqrt{2}$ from left bottom to right top ($\xi = \eta$) on the map. The source intensity, $|Q|$, up to -10 dB from the peak is then integrated in space for each source position to calculate both intensity and centroid.

Figure 2 shows the results for the case corresponding to Fig. 1a, where Δ denotes the error of the designated quantity. All the

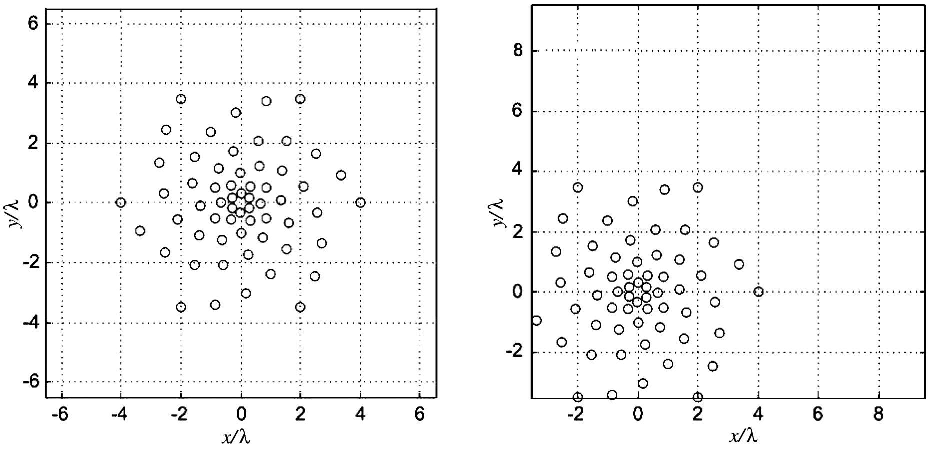

a) b)

Fig. 1 Microphone positions relative to the noise-source map for model problems: a) source map centered at (0, 0); b) centered at (3λ, 3λ).

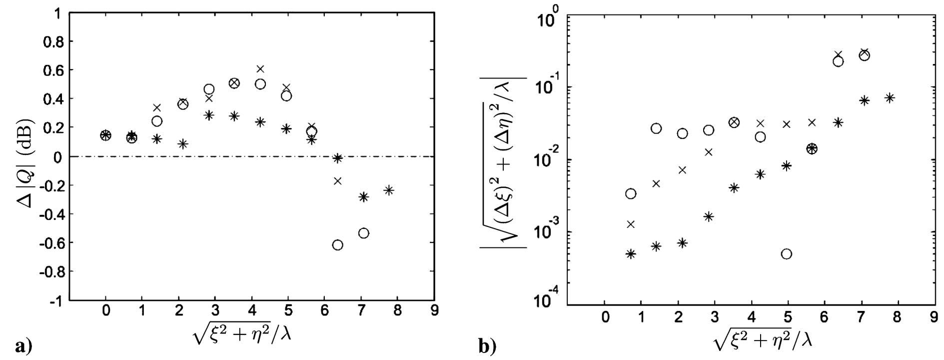

a) b)

Fig. 2 Comparison of the source-detection accuracy based on a monopole: the circle indicates DAMAS2, the x indicates the first-order correction of the proposed algorithm, and the asterisk is the second-order correction of the proposed algorithm. The microphone positions correspond to Fig. 1a. Graphs of a) discrepancy of the source intensity, and b) discrepancy of the source position.

algorithms detect the source intensity within 1 dB discrepancy. DAMAS2 abruptly deteriorates $\Delta|Q|$ beyond 6λ (then fails to localize the source beyond about 7λ), and the proposed algorithm with the first-order correction hardly improves the accuracy. In contrast, that with the second-order correction retains higher accuracy up to nearly the corner of the domain. The source centroid detected with the second-order correction is approximately 1 order of magnitude more accurate compared with DAMAS2 or the first-order correction, and its discrepancy gradually increases with the distance. As a result, the usable domain extends by as much as 2λ in this example.

When the source position is away from the map center, corresponding to Fig. 1b, the benefit and the limitation of the proposed algorithms become clearer. Near the center of the array, the nature of the point-spread function behaves as a local optimum. Therefore, the proposed algorithm with the first-order correction significantly overestimates the source intensity at smaller $\sqrt{\xi^2+\eta^2}$ in Fig. 3a, unlike the other two algorithms. At a greater distance from the array center, DAMAS2 rapidly drops the detected intensity beyond 7λ, while the proposed algorithm with the second order can estimate the source intensity with better accuracy, even close to 10λ. The trends of the detected source position in Fig. 3b similarly exhibit the

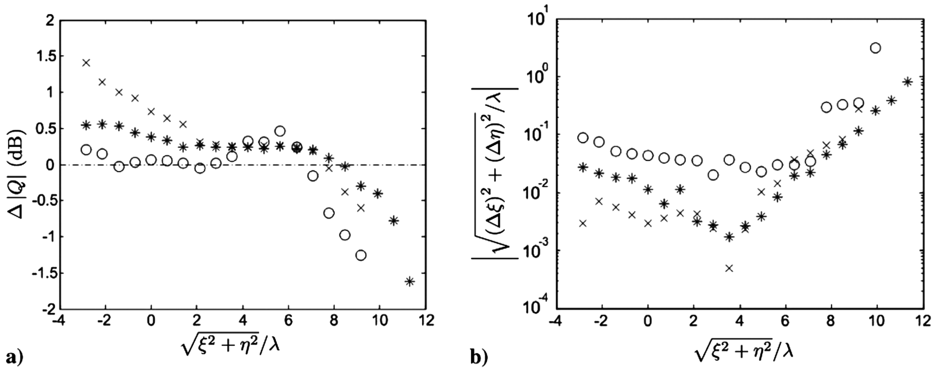

Fig. 3 Comparison of the source-detection accuracy based on a monopole. The microphone positions correspond to Fig. 1b. Symbols are the same as Fig. 2. Negative $\sqrt{\xi^2+\eta^2}$ signifies the $\xi<0$, $\eta<0$ domain. Graphs of a) discrepancy of the source intensity, and b) discrepancy of the source position.

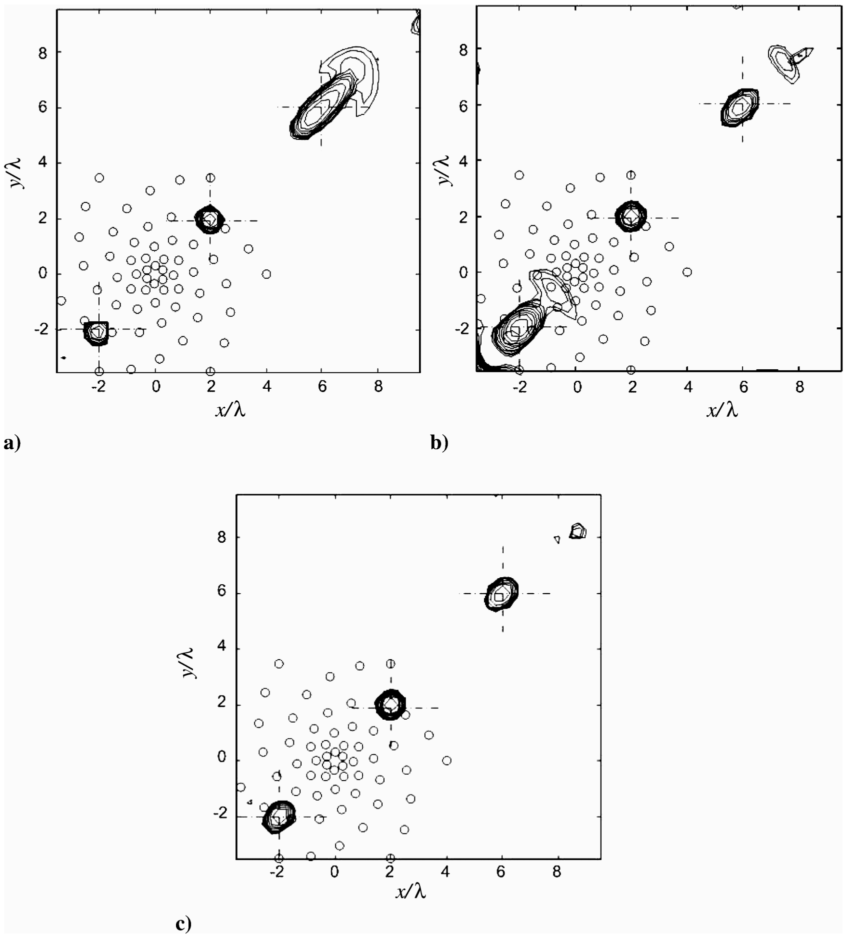

Fig. 4 Comparison of monopole responses. The microphone distribution corresponds to Fig. 1b. Contours of a monopole located at $(\xi,\eta)=(-2,-2)$, (2, 2) and (6, 6), denoted by dotted crosses, are overlaid in each figure (three cases are separately computed) in 10 dB range from the peak with 1 dB interval. Graphs of a) DAMAS2, b) proposed algorithm with the first-order correction, and c) second-order correction.

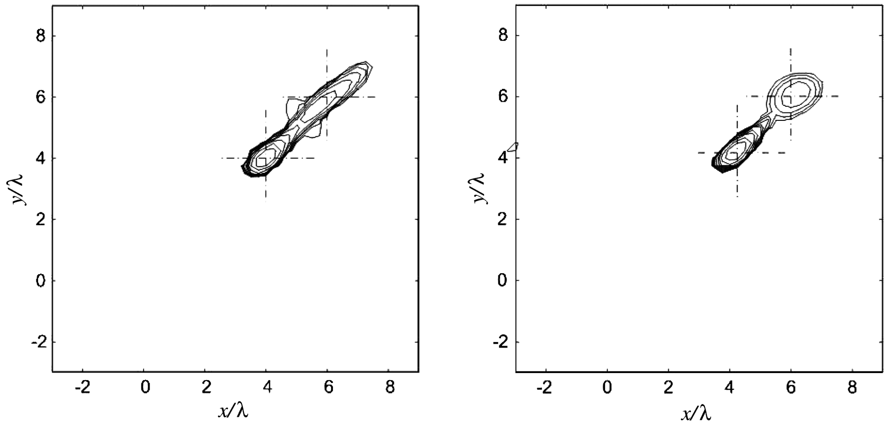

a) b)

Fig. 5 Source maps of two adjacent incoherent sources with the same intensity. Drawing patterns are the same as Fig. 4, and the microphone positions correspond to Fig. 1b. One source is located at $(\xi, \eta) = (6, 6)$. Graphs of a) DAMAS2 with the other source at $(\xi, \eta) = (4, 4)$, and b) second-order correction with the other source at $(\xi, \eta) = (4.1, 4.1)$.

superiority of the higher-order correction. In particular, the second-order correction is most accurate near the map center (not the array center), where the point-spread function is defined.

The proposed algorithm can also suppress distortion of lobe shapes on the source map. Figure 4 compares monopole contours on the source map between DAMAS2 and the proposed algorithms. When the source exists at the center of the map, all source maps show a sharp peak. However, the spots for the sources away from the center tend to elongate, for example, at $(\xi, \eta) = (6\lambda, 6\lambda)$ using DAMAS2 in Fig. 4a and at $(\xi, \eta) = (-2\lambda, -2\lambda)$ using the first-order correction in Fig. 4b, causing distortion of contour maps. In contrast, the second-order correction of the proposed algorithm produces relatively consistent lobes regardless of the source position in Fig. 4c. Thus, the second-order correction allows us to expand the size of a source map or to locate it away from the array center.

In addition, the resolvable distance of two adjacent sources is examined. One monopole is located at $(\xi, \eta) = (6\lambda, 6\lambda)$, and the other incoherent one with the same intensity is moved diagonally with $\sqrt{2}\lambda$ increment to observe the minimum separation distance. In the DAMAS2 map, the second peak is created when the second source is located at $(\xi, \eta) = (4.0\lambda, 4.0\lambda)$ or closer to the center, as displayed in Fig. 5a. Using the second-order correction, the second peak becomes discernible at a closer distance, i.e., $(\xi, \eta) = (4.7\lambda, 4.7\lambda)$, not shown; however, to locate the second peak within the 6 dB range at a reasonable position, it must be located at $(4.1\lambda, 4.1\lambda)$ or closer to the center, as shown in Fig. 5b. Because the evolution of the lobe patterns is different between the two algorithms, it is difficult to conclude the superiority of the proposed algorithm.

Table 1 compares elapsed computational times for a single map in this model problem. For reference, it lists the results of two different grid points (105×105 in addition to 53×53). The total time includes calculation of a point-spread function, its derivatives, filtering and discrete Fourier transforms in addition to the iteration part. For both iteration part and total time, the first-order correction takes about twice and the second-order correction about 4 times as long as DAMAS2. Note that the extension to the third-order correction requires 20 additional terms in (6) and would increase the computational cost by an order of magnitude relative to DAMAS2.

IV. Example of Source Maps Using Test Data

Finally, Fig. 6 compares noise-source maps processing a model-scale test of a Boeing 747-400 in the QinetiQ five-meter closed wind tunnel. In this example, the microphone array was located far from the airplane center. In both maps, the landing-gear, flap-edge and leading-edge-slat (one side only) noise components are captured. In

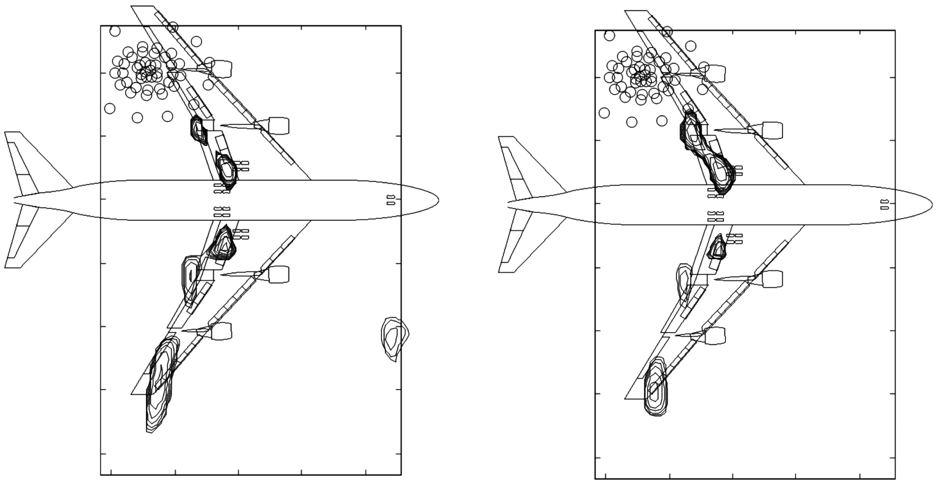

a) b)

Fig. 6 Comparison of noise-source maps for a model-scale Boeing 747-400 at 154 Hz (corresponding full scale). Contours levels are the same as Fig. 4. Microphone distributions are overlaid. Graphs of a) DAMAS2, and b) second-order correction of the proposed algorithm.

Table 1 Comparison of elapsed computational times. Computation was performed using MATLAB with a single-processor PC. Unit is second

Algorithms	DAMAS2	First-order correction	Second-order correction
Time for 50 iterations (53 × 53)	0.14	0.30	0.61
Total time (53 × 53)	0.54	1.20	2.00
Time for 50 iterations (105 × 105)	0.38	0.67	1.21
Total time (105 × 105)	1.29	3.03	5.03

Fig. 6b, as the source close to the outboard edge of the inboard flap on the upper side is identified as a strong one, it appears to be merged with the landing-gear noise (it should be noted that these noise sources are highly directive). But, in general, the lobes in the DAMAS2 map are elongated at farther distances, particularly at the leading-edge slat, while more compact lobes are produced using the proposed algorithm with the second-order correction.

V. Conclusions

This study proposes an algorithm that extends the capability of DAMAS2 with a point-spread function weakly varying in space. By expanding the monopole response in a Taylor series and retaining up to the second-order terms, the proposed algorithm can increase the detection accuracy in terms of the source intensity and position. The drawback is the extra computational time required for derivative terms of the point-spread function, which is mostly performed before iteration. The resultant computational time is a few times longer than that for DAMAS2, but is still the same order of magnitude faster than the original DAMAS.

Acknowledgment

The author greatly appreciates J. V. Larssen, L. Brusniak, and R. W. Stoker for productive discussions, editorial suggestions and data-migration support.

References

[1] Brooks, T. F., and Humphreys, W. M., "A Deconvolution Approach for the Mapping of Acoustic Sources (DAMAS) Determined from Phased Microphone Arrays," *Journal of Sound and Vibration*, Vol. 294, Nos. 4–5, 2006, pp. 856–879.
doi:10.1016/j.jsv.2005.12.046

[2] Dougherty, R. P., "Extension of DAMAS and Benefits and Limitations of Deconvolution in Beamforming," AIAA Paper 2005-2961, May 2005.

[3] Ehrenfried, K., and Koop, L., "Comparison of Iterative Deconvolution Algorithms for the Mapping of Acoustic Sources," *AIAA Journal*, Vol. 45, No. 7, 2007, pp. 1584–1595.
doi:10.2514/1.26320

A. Lyrintzis
Associate Editor